# Numerical Calculation of the Electromagnetic Expulsive Force upon Nonmetallic Inclusions in an Aluminum Melt: Part I. Spherical Particles

DA SHU, BAO-DE SUN, JUN WANG, TIAN-XIAO LI, ZHEN-MING XU, and YAO-HE ZHOU

The finite-element method was employed to explore the electromagnetically engendered fluid streaming around a spherical inclusion particle suspended in aluminum melt, and numerical integration of the pressure over the particle surface was made to calculate the electromagnetic expulsive force exerted on the particle. It was found that convection flows with four cells appear around the particle along the direction of the electromagnetic force. The change of pressure gradient is confined within the thin-skin layer around the particle, while the perturbance of the velocity field widely spreads out. Compared with the theoretical results derived from the analytical method, the numerical results agree well in the range of small particle sizes or low-intensity force densities. For large particle sizes or high-intensity force densities, the calculated expulsive force is only a little bit larger than the theoretical result. The influence of a boundary effect and proximity effect on the electromagnetic expulsive force is insignificant, except for a slight increase in the expulsive force when the particle approaches a boundary or other particles.

## I. INTRODUCTION

THE presence of nonmetallic inclusions in aluminum has an adverse effect on the reliability and performance of the end product and may lead to increased porosity, a drastic reduction in mechanical properties, poor machinability, loss of fluidity, and lack of pressure tightness.[1–3] With the increasing trends toward high quality, down-gaging, and recycling of aluminum products, the demand for improved melt cleanliness levels continues to grow. As a result, the elimination of inclusions is central to both the primary and secondary aluminum industries.

It is believed that inclusions down to 5 $\mu$m in size[4] and of several parts per million in volume[5] are harmful to premium products. Although a number of melt-refining methods for the removal of inclusions prior to casting exist, efficient and consistent removal of small inclusions is very difficult to attain.[6] Based on the basic separation mechanisms, gravity sedimentation may be effective for inclusions larger than 90 to 100 $\mu$m. The flotation technique may be effective for inclusions of up to about 30 to 40 $\mu$m.[7] Removal of inclusions of less than 30 $\mu$m may be accomplished by filtration using ceramic foam filters,[5] but with limited and controversial filtration efficiency.[1,8]

Electromagnetic separation can, by comparison, remove even micrometer-sized inclusions, in principle, by using high-intensity force fields at an almost constant rate.[9,10] The concept of this innovative method is based on the following phenomenon: when a nonconductive particle is immersed in an enclosed conductive fluid traversed by a homogeneous electric current and a homogeneous magnetic field perpendicular to that current, it will experience a resultant expulsive force in the opposite direction of the electromagnetic force exerted on the fluid itself, partly due to the quasi-buoyant surface force and partly to a hydrodynamic force arising from the liquid streaming in its surrounding area, owing to the distortion of the electromagnetic field.[11,12] Since electromagnetic separation makes use of the difference in electrical conductivity between the inclusion particle and the melt, rather than the density difference, it is particularly appropriate for the case of molten aluminum, in which inclusions suspended are very similar to the melt in density.[13,14]

While substantial research have been done on the different types of electromagnetic separators[9,15–19] and the effects of various operating parameters on the separation efficiency,[20] which clearly demonstrates the potential and effectiveness of electromagnetic separation, fundamental work concerning the origin of the electromagnetic expulsive force remains scarce. In the limited previous studies, Leenov and Kolin,[12] Marty and Alemany,[21] and Korovin[22] derived the theoretical expression of the electromagnetic expulsive force for some simple cases, such as a spherical particle and an infinitely long cylindrical particle whose axis is parallel to the electric field, the magnetic field, or the force field. Nevertheless, the simplification that the inertial terms in the flow-momentum equations are neglected has been made. The end corrections for the finite cylinder, as well as the effects of the particle shape and orientation, have not been considered. Furthermore, the influences of the proximity effect between two particles, and of the boundary effect when a particle approaches or leaves, are still to be investigated.

In order to overcome the difficulties associated with the analytical method, the finite-element method is employed in this article to evaluate the effect of the electromagnetically engendered streaming of the fluid, and numerical integration of the pressure over the particle surface is made to calculate the electromagnetic expulsive force. Particles of various shapes and orientations are, thus, considered, as well as the proximity effect and the boundary effect. The obtained numerical results are compared with the theoretical results

DA SHU and TIAN-XIAO LI, Doctoral Candidates, BAO-DE SUN and YAO-HE ZHOU, Professors, and JUN WANG and ZHEN-MING XU, Associate Professors, are with the School of Materials Science and Engineering, Shanghai Jiao Tong University, Shanghai 200030, People's Republic of China.

Manuscript submitted February 3, 2000.

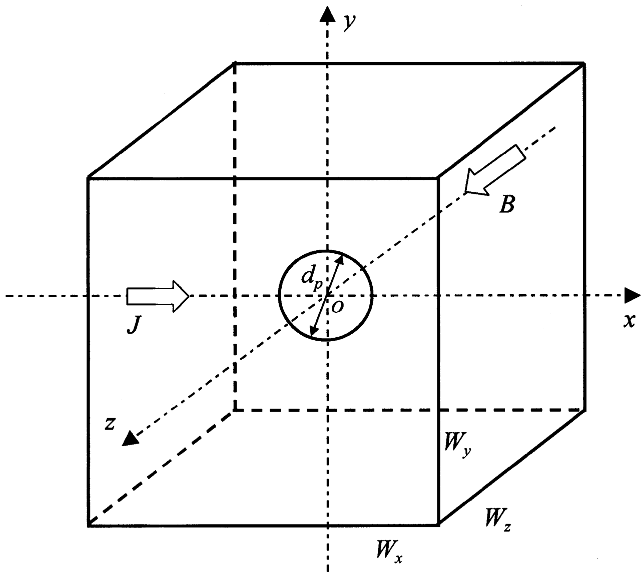


Fig. 1—The sketch of the physical model.

and some experimental data of other workers. In part I of this two-part series of articles, we will first deal with the case of a spherical particle.

## II. NUMERICAL METHODS

The physical model of the problem is sketched in Figure 1. The calculated region is composed of a $W_x \times W_y \times W_z$ block, representing a conductive fluid, and a sphere in the origin, representing an insulating particle. A uniform electric-current density ($J$) is imposed along the $x$-axis, and a uniform magnetic field ($B$) is imposed along the $z$-axis.

### A. *Assumptions*

As the aluminum melt and the inclusions suspended in it, which are typically 1 to 30 $\mu$m in size,[1,7] are our main concerns, the following assumptions were made.

(1) Distortion of the electric field and the engendered disturbance of the fluid are confined to the limited region surrounding the particle. The outer boundary of the fluid is assumed to be far enough to remain unaffected.
(2) The fluid flow is characterized by a small magnetic Reynolds number, *i.e.*, $R_m = \mu_e \sigma_f U d_p << 1$, where $\mu_e$ and $\sigma_f$ are the magnetic permeability and the electrical conductivity of the fluid, respectively, $U$ is the characteristic velocity, and $d_p$ is the particle diameter. Thus, the flow field has no effect on the electromagnetic field.
(3) The magnetic field induced by the applied electric current is neglected.
(4) The flow is laminar and in steady state.

### B. *Governing Equations*

1. *Electric field*

The basic equation for the electric-current field is Laplace's equation for the electric potential,

$$\nabla^2 \phi = 0 \qquad [1]$$

where $\phi$ is the electric potential. The distribution of the electric-current density can be obtained from

$$\mathbf{J} = -\sigma \nabla \phi \qquad [2]$$

where $\sigma$ is the electrical conductivity, and $\mathbf{J}$ is the electric-current-density vector.

2. *Fluid flow*

The steady-state fluid-flow equations can be represented by the Navier–Stokes equations,

$$\rho_f \mathbf{v} \cdot \nabla \mathbf{v} = -\nabla p + \mathbf{f} + \mu_f \nabla^2 \mathbf{v} \qquad [3]$$

and the continuity equation.

$$\nabla \cdot \mathbf{v} = 0 \qquad [4]$$

where $\rho_f$ and $\mu_f$ are the density and the kinetic viscosity of the fluid, respectively, $\mathbf{f}$ is the Lorentz force acting on a unit-volume fluid.

### C. *Boundary Conditions*

For Laplace's equation (Eq. [1]), a finite potential value is applied on the left face of the outer boundary, while a zero value is specified on the opposite face to impose a current density along the $x$-axis. At the fluid-particle interface, continuity of the normal component of the electric-current density and continuity of the potential are satisfied:

$$J_{fn} = J_{pn} \text{ or } \sigma_f \frac{\partial \varphi_f}{\partial n} = \sigma_p \frac{\partial \varphi_p}{\partial n} \qquad [5]$$

$$\phi_f = \phi_p \qquad [6]$$

The boundary conditions for the fluid flow are no-slip conditions at the particle surface and a zero velocity at the outer boundary, as assumed in Section II–A.

### D. *Meshing and Solutions*

As described previously, the outer boundary should be far enough from the particle in order to ensure the calculation precision. However, too large a domain of calculation would lead to a significant increase in the number of elements and the computational expense. In this study, the outer boundary is specified as $W_x = W_y = W_z = 50\ d_p$. The whole region is meshed in tetrahedron elements, to an extent that further mesh refinement only gives a minor difference in the results.

The electric field is first calculated by solving Eq. [1], and the Lorentz force acting on the fluid is calculated according to

$$f_x = J_{fy} B_z, \quad f_y = -J_{fx} B_z \qquad [7]$$

where $J_{fx}$ and $J_{fy}$ are the $x$- and $y$-component of the electric-current density inside the fluid, respectively. The obtained Lorentz force is then substituted into the volume force term ($\mathbf{f}$) of the Navier–Stokes equations (Eq. [3]) to compute the fluid velocity and pressure change, combined with the continuity equation (Eq. [4]). The above solutions were performed using ANSYS, a commercial finite-element analysis software, on a personal computer platform.

### E. *Calculation of the Expulsive Force*

By theory, the particle is subjected to the surface force exerted by the fluid and the electromagnetic volume force.

**Table I. Property Values Used for the Calculations**

| | Electrical Conductivity (S/m) | Density (kg/m$^3$) | Viscosity (Pa · s) |
|---|---|---|---|
| Fluid | $2.95 \times 10^6$ | $2.37 \times 10^3$ | $2.5 \times 10^{-3}$ |
| Particle | $10^{-10}$ | — | — |

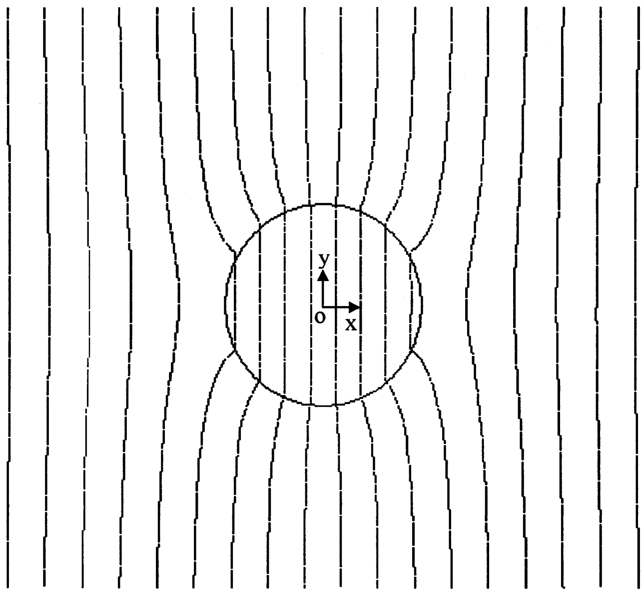


Fig. 2—Isopotential lines around the particle in the *xoy* plane, $J = 1 \times 10^6$ A/m$^2$, $B = 1$ T, and $d_p = 20$ $\mu$m.

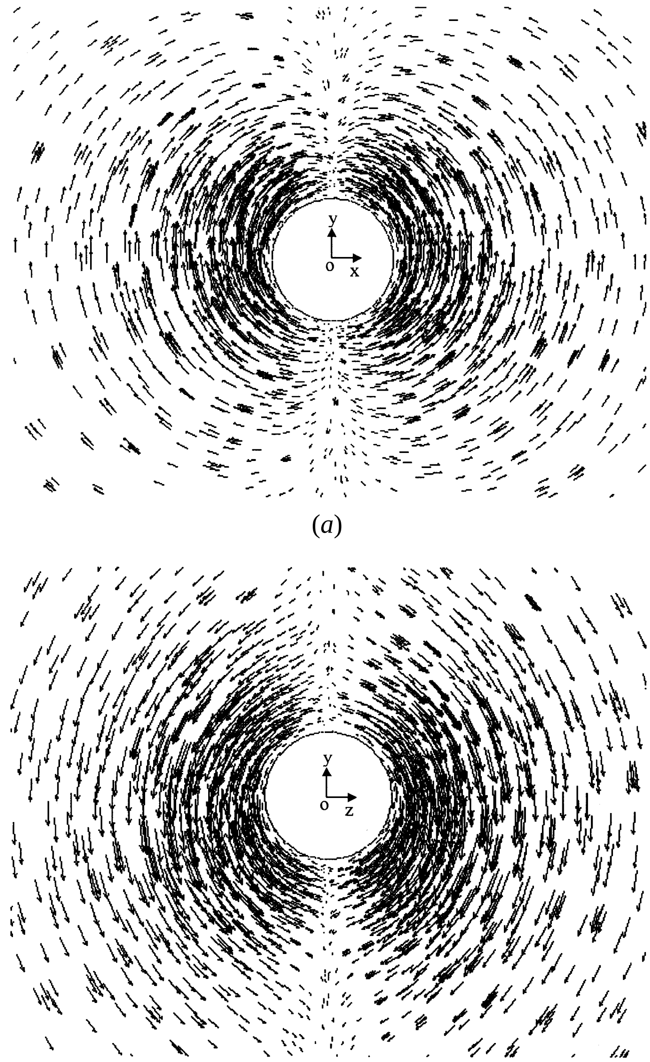


Fig. 3—Vector diagram of the fluid velocities (*a*) in the plane of *xoy* and (*b*) in the plane of *yoz*, $J = 1 \times 10^6$ A/m$^2$, $B = 1$ T, and $d_p = 20$ $\mu$m.

For insulating particles such as nonmetallic inclusions, the electromagnetic volume force vanishes. The surface force ($\mathbf{F}_s$) will be caused by two effects, the ordinary pressure contribution and the viscous stress due to motion of the fluid, and can be written as

$$\mathbf{F}_s = \iint (p\mathbf{ds} + \mathbf{T} \cdot \mathbf{ds}) \qquad [8]$$

where $\mathbf{T} = 2\ \mu_f\ (1/2(\partial v_i/\partial x_j + \partial v_j/\partial x_i))$ is the deviatoric stress tensor. In this study, the latter part of the integrand is neglected due to the special flow pattern that will be seen in the next section. The electromagnetic expulsive force on the particle is obtained by numerical integration of the pressure over the particle surface, based on the calculated results of fluid flow.

## III. RESULTS AND DISCUSSION

### A. *Flow Pattern*

The property values used for the calculations are listed in Table 1. Figure 2 plots the calculated isopotential lines of the electric field around the particle in the *xoy* plane. The deformation of the electric field by the particle can be clearly seen, and the engendered inhomogeneity of the electromagnetic force field gives rise to the streaming of the fluid. Figure 3 shows the vector diagram of the fluid velocities around the particle in the sections of *xoy* and *yoz*. It can be seen that the flow pattern is quite different from that of the creeping flow past a sphere. The fluid flows in the positive direction of the *y*-axis in the *xoy* plane (Figure 3(a)), while it circulates in the negative direction of the *y*-axis in the *yoz* plane (Figure 3(b)). Thus, convection flows with four cells appear around the particle along the direction of the electromagnetic force, which is depicted in Figures 4 and 5. It can be deduced from such a flow pattern that the total frictional force due to fluid shear stress at the particle surface can be considered to be negligible.

The evolution of the velocity with radial distance along different straight lines is shown in Figure 6. The contour of pressure around the particle is depicted in Figure 7. It can be seen that the change of pressure gradient is confined within the thin-skin layer around the particle, while the perturbance of the velocity field widely spreads out.

### B. *Numerical Results vs Theoretical Results*

The steady-flow Navier–Stokes equations may be greatly simplified by omission of the $\mathbf{v} \cdot \nabla\mathbf{v}$ inertia term. The theoretical expressions for fluid velocities and pressure derived by Leenov and Kolin[12] are as follows:

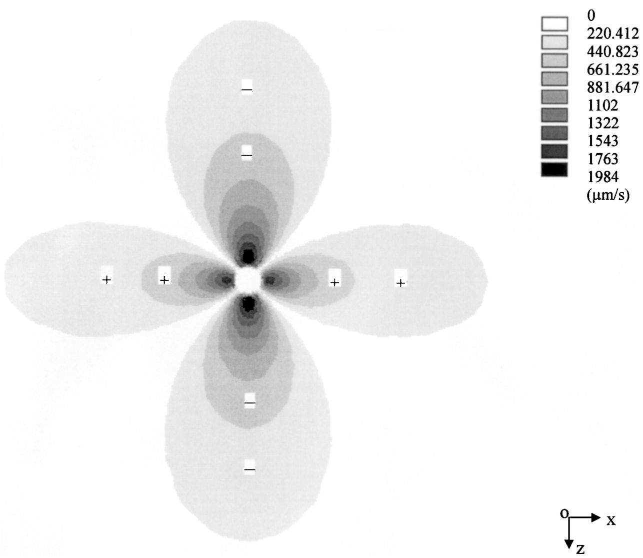


Fig. 4—Sectional velocity profile of the convection flows with four cells in the *xoz* plane, $J = 1 \times 10^6$ A/m$^2$, $B = 1$ T, and $d_p = 20$ $\mu$m (the direction of velocity is illustrated by signs).

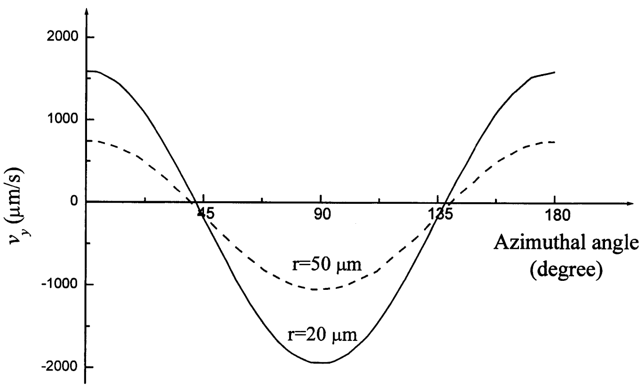


Fig. 5—Variation of the *y*-component velocity with the azimuthal angle in the *xoz* plane, $J = 1 \times 10^6$ A/m$^2$, $B = 1$ T, and $d_p = 20$ $\mu$m.

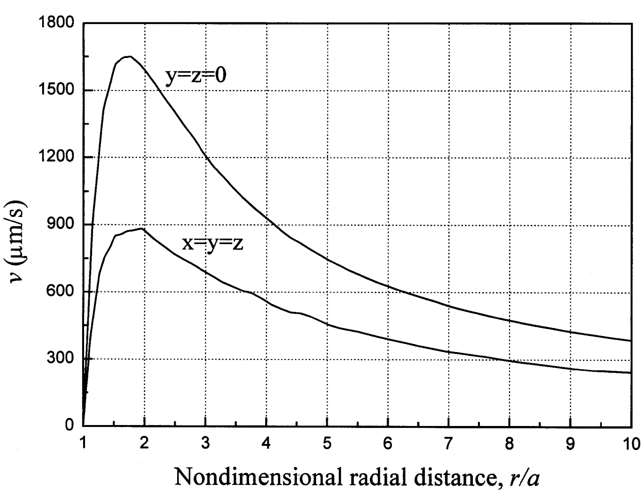


Fig. 6—Evolution of the velocity with the nondimensional radial distance, $J = 1 \times 10^6$ A/m$^2$, $B = 1$ T, and $d_p = 20$ $\mu$m.

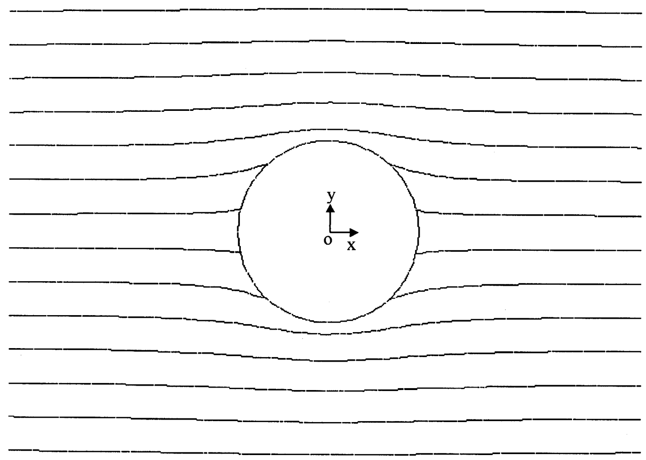


Fig. 7—Distribution of pressure around the particle in the *xoy* plane, $J = 1 \times 10^6$ A/m$^2$, $B = 1$ T, and $d_p = 20$ $\mu$m.

$$\mathbf{v} = \frac{JB}{8\,\mu_f}\frac{a^3}{r^3}\left(\frac{a^2}{r^2} - 1\right)(xy\mathbf{e}_x + (z^2 - x^2)\mathbf{e}_y - yz\mathbf{e}_z) \quad [9]$$

$$p = -\left(1 - \frac{1}{4}\cdot\frac{a^3}{r^3}\right)JBy \quad [10]$$

where $a$ is the radius of the sphere, and $\mathbf{e}_x$, $\mathbf{e}_y$, and $\mathbf{e}_z$ are the unit vectors in the direction of increase of the corresponding coordinates. By expressing Eq. [9] in a spherical coordinate system, we can find the maximum velocity inside the fluid:

$$V_{\max} = \frac{JB}{8\,\mu_f}\cdot\frac{2}{3\sqrt{3}}\cdot a^2 \quad [11]$$

at $(x = \pm\sqrt{3}\,a, y = 0, z = 0)$ or $(x = 0, y = 0, z = \pm\sqrt{3}\,a)$.

From Eqs. [9] and [10], the electromagnetic expulsive force can be obtained by calculating the integral on the right-hand side of Eq. [8]. It was found that the latter part of the integrand will be averaged over all directions on integrating over the surface of the sphere, and the contribution by the viscous stress to the total force vanishes exactly.[12] According to Leenov and Kolin's therory,[12] the electromagnetic expulsive force exerted on an insulating particle takes the following form:

$$\mathbf{F} = \mathbf{F}_s = \frac{3}{4}JBV\mathbf{e}_y \quad [12]$$

where $V = 1/6\ \pi d_p^3$ is the volume of the particle, and $JBV$ represents the electromagnetic force exerted on the displaced volume of fluid.

The validity of the previous theory may be approximately evaluated by the dimensional analysis. The limitation given by Leenov and Kolin[12] is as follows:

$$JBa^3 \cdot \rho_f << \mu_f^2 \quad [13]$$

Using the property values in Table I, if $JB = 1 \times 10^6$ N/m$^3$ or $JB = 1 \times 10^7$ N/m$^3$, we found the previous condition equivalent to $d_p << 28$ $\mu$m or $d_p << 13$ $\mu$m, respectively. Therefore, the application of the theory to large particles or small particles under a high-intensity force field may be questionable.

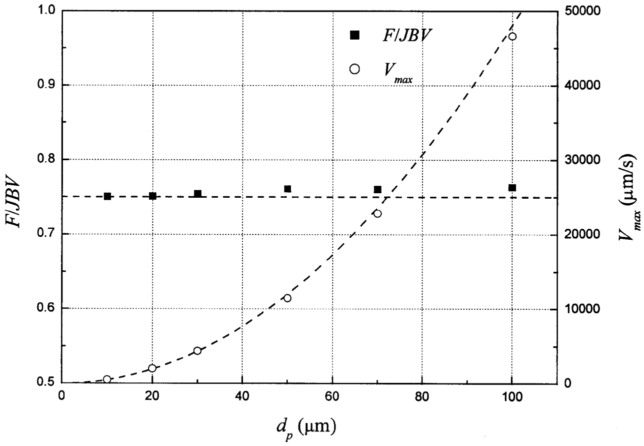


Fig. 8—Variation of electromagnetic expulsive force and the maximum velocity with the particle diameter, $J = 1 \times 10^6$ A/m$^2$, and $B = 1$ T (theoretical results are drawn in dashed lines for comparison).

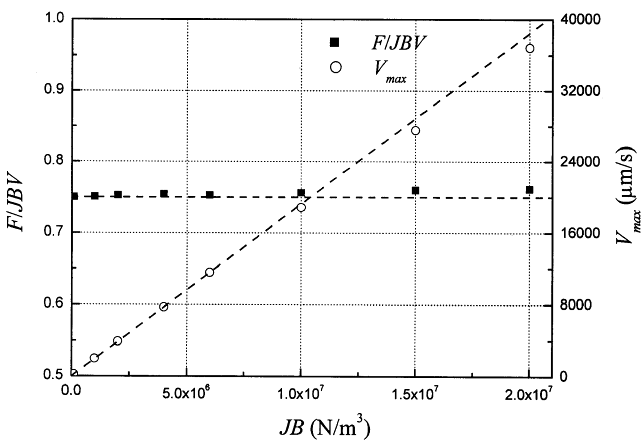


Fig. 9—Variation of electromagnetic expulsive force and the maximum velocity with the imposed electromagnetic force density, $d_p = 20$ $\mu$m (theoretical results are drawn in dashed lines for comparison).

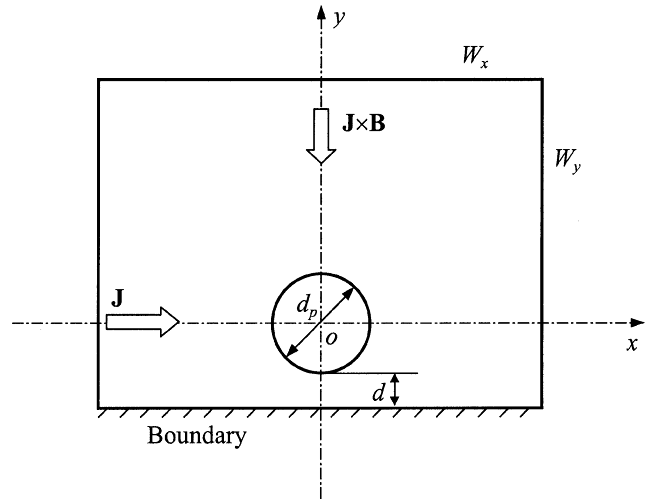


Fig. 10—Sketched model for calculation of boundary effect.

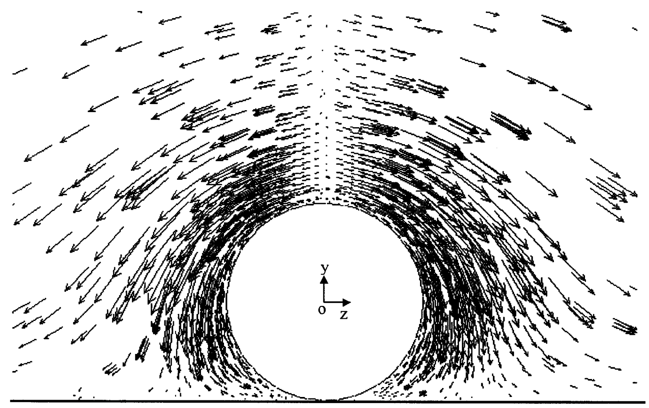


Fig. 11—Vector diagram of the fluid velocities in the plane of *yoz*, $J = 1 \times 10^6$ A/m$^2$, $B = 1$ T, $d_p = 20$ $\mu$m, and $d = 0$.

Figures 8 and 9 show the variation of the calculated values of $F/JBV$ and $V_{max}$ with the particle diameter and the imposed electromagnetic force density, respectively. The theoretical results are also drawn in dashed lines. It can be seen that the numerical results agree well with the theory in the range of small particle sizes or low-intensity force densities as we expect. For large particle sizes or high-intensity force densities, the calculated expulsive force is only a little bit larger than the theoretical result, while the difference between the calculated values of the maximum velocity and the theoretical results is also small.

It should be pointed out that the effect of the inertial force is not equal throughout the flow regime. In the regime that is immediately adjacent to the particle's surface, where viscosity is predominant, the inertial force is negligible. However, as the viscous effect declines faster than the inertial effect, the neglect of the inertial force may be inaccurate in the regime far away from the particle. However, in our problem the fluid is at standstill at the outer boundary. Besides, as previously mentioned, the change of the pressure gradient is confined within the thin-skin layer around the particle, where the viscous effect is predominant. It can be deduced that Leenov and Kolin's theory may hold for a wider range than that restricted by the limitation in Eq. [13] from the force's point of view.

## C. *Boundary Effect*

The model for calculation of the boundary effect is shown in Figure 10, where the particle is expulsed to leave the boundary. The outer boundary is set as $W_x = W_z = 50\ d_p$ and $W_y = 25\ d_p + d_p/2 + d$, where $d$ is the distance between the particle and the boundary. The governing equations as well as boundary conditions are the same as before, and the numerical methods described previously still apply. The calculated velocity field and pressure diagram are depicted in Figures 11 and 12, respectively. The influence of the boundary effect on the electromagnetic expulsive force is shown in Figure 13. When compared with the previously calculated results, although the velocity field is considerably altered by the boundary, the pressure distribution and the electromagnetic expulsive force are less affected.

By reversing the imposed electric current, the effect when a particle approaches a boundary can be easily investigated. The evolution of the expulsive force with $d/d_p$, in this case, is found to be exactly the same as that shown in Figure 13. It can be seen that the expulsive force increases as the particle

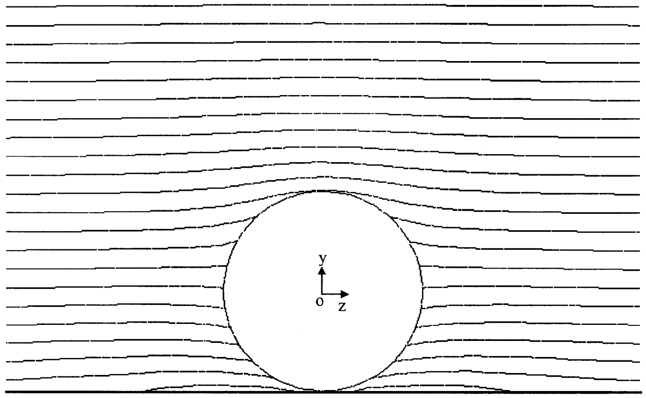

Fig. 12—Pressure diagram around the particle in the *yoz* plane, $J = 1 \times 10^6$ A/m$^2$, $B = 1$ T, $d_p = 20$ $\mu$m, and $d = 0$.

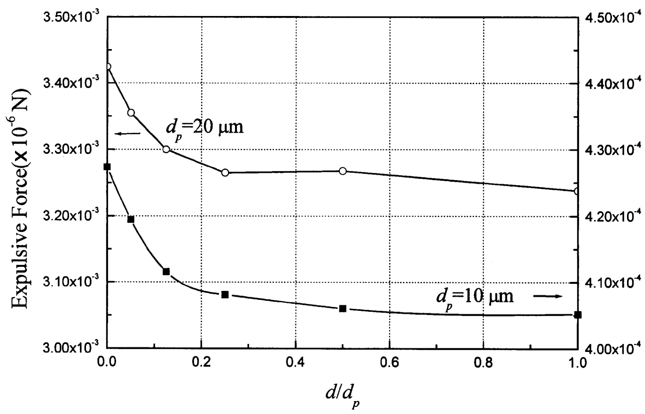

Fig. 13—Influence of boundary effect on the electromagnetic expulsive force, $J = 1 \times 10^6$ A/m$^2$, and $B = 1$ T.

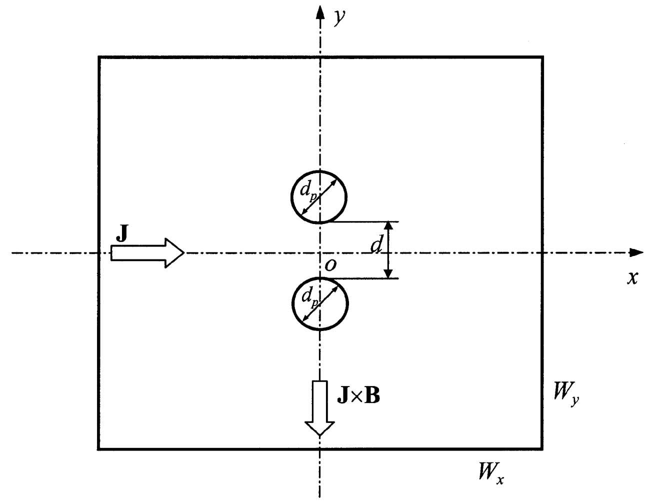

Fig. 14—Sketched model for calculation of proximity effect.

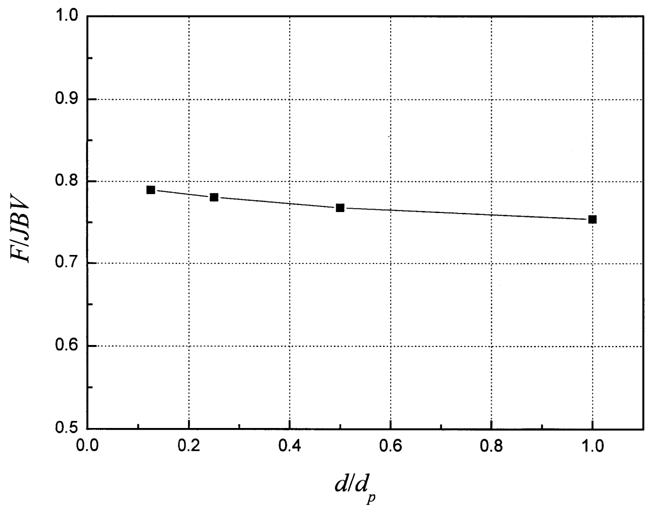

Fig. 15—Influence of proximity effect on the electromagnetic expulsive force, $J = 1 \times 10^6$ A/m$^2$, $B = 1$ T, $d_p = 20$ $\mu$m.

approaches the boundary. When the particle reaches the boundary, the ratio $F/JBV$ is above 0.8. Therefore, the boundary effect is favorable for the separation of inclusions, as it promotes the fix of inclusions at the boundary in kinetics.

### D. *Proximity Effect*

The previous discussions are all concerned with a single particle. When two particles are near enough, changes in the flow field as well as in the electromagnetic expulsive force can be expected. This proximity effect between two particles is calculated based on the model illustrated in Figure 14. It is found that the expulsive forces exerted on the two spheres are almost same. Figure 15 gives the calculated $F/JBV$ value as a function of $d/d_p$, where $d$ is the distance between the two spheres. Somewhat like the boundary effect, the expulsive force increases with the decrease of the distance between the two particles.

## IV. CONCLUSIONS

The finite-element method has been used in this article to evaluate the effect of electromagnetically engendered fluid streaming on the electromagnetic expulsive force exerted on a spherical particle. The following conclusions are drawn.

1. Convection flows with four cells appear around the particle, due to the deformation of the electric field by the insulating particle.
2. The change of pressure gradient is confined within the thin-skin layer around the particle, while the perturbance of the velocity field widely spreads out.
3. The numerical results agree well with the analytical results in the range of small particle sizes or low-intensity force densities. For large particle sizes or high-intensity force densities, the calculated expulsive force is only a little bit larger than the theoretical result.
4. The influence of the boundary effect and proximity effect on the electromagnetic expulsive force is insignificant, except for a slight increase in the expulsive force when the particle approaches a boundary or other particles.

## ACKNOWLEDGMENTS

This work is supported by the National Natural Science Foundation of China (Grant No. 59871029) and the National

Key Fundamental Research Project (973) (No. G1999064900).

## NOMENCLATURE

| | |
|---|---|
| $a$ | particle radius |
| $B$, $B_z$ | imposed magnetic flux density |
| $d$ | distance between the particle and a boundary or another particle |
| $d_p$ | particle diameter |
| $\mathbf{F}$ | electromagnetic expulsive force |
| $f$ | Lorentz force acting on fluid |
| $J$ | imposed electric current density |
| $p$ | pressure |
| $\mathbf{T}$ | deviatoric stress tensor |
| $\mathbf{v}$ | velocity vector |
| $V$ | volume of the particle |
| $V_{\max}$ | the maximum velocity inside the fluid |
| $W_x$, $W_y$, $W_z$ | outer boundary of fluid |

Greek Symbols

| | |
|---|---|
| $\mu_e$ | magnetic permeability |
| $\mu$ | kinetic viscosity |
| $\rho$ | density |
| $\sigma$ | electrical conductivity |
| $\phi$ | electric potential |

Subscripts

| | |
|---|---|
| $f$ | fluid |
| $p$ | particle |
| $n$ | normal direction |

## REFERENCES


1. G.K. Sigworth, S. Shivkumar, and D. Apelian: *Am. Foundrymen's Soc. Trans.*, 1989, vol. 97, pp. 811-24.
2. L. Liu and F.H. Samuel: *J. Mater. Sci.*, 1998, vol. 33, pp. 2269-81.
3. G. Laslaz and P. Laty: *Am. Foundrymen's Soc. Trans.*, 1991, vol. 99, pp. 83-90.
4. A.G. Szekely: *Metall. Trans. B*, 1976, vol. 7B, pp. 259-70.
5. D. Apelian and R. Mutharasan: *J. Met.*, 1980, Sept., pp. 14-19.
6. F. Frisvold, T.A. Engh, S.T. Johansen, and T. Pedersen: in *Light Metals 1992*, E.R. Cutshall, ed., TMS, Warrendale, PA, 1991, pp. 1125-32.
7. S. Shivkumar, L. Wang, and D. Apelian: *JOM*, 1991, Jan., pp. 26-32.
8. R.A.P. Fielding: *Light Met. Age*, 1996, Oct., pp. 46-59.
9. N. El-Kaddah, A.D. Patel, and T.T. Natarajan: *JOM*, 1995, May, pp. 46-49.
10. A.D. Patel and N. El-Kaddah: in *Light Metals 1997*, R. Huglen, ed., TMS, Warrendale, PA, 1997, pp. 1013-18.
11. A. Kolin: *Science*, 1953, vol. 117, pp. 134-37.
12. D. Leenov and A. Kolin: *J. Chem. Phys.*, 1954, vol. 22, pp. 683-88.
13. P.N. Crepeau: *Modern Casting*, 1997, July, pp. 39-41.
14. D.V. Neff and P.V. Cooper: *Am. Foundrymen's Soc. Trans.*, 1990, vol. 98, pp. 579-84.
15. J.-P. Park, A. Morihira, K. Sassa, and S. Asai: *Tetsu-to-Hagané*, 1994, vol. 80 (5), pp. 31-36.
16. Y. Tanaka, K. Sassa, K. Iwai, and S. Asai: *Tetsu-to-Hagané*, 1995, vol. 81 (12), pp. 12-17.
17. F. Yamao, K. Sassa, K. Iwai, and S. Asai: *Tetsu-to-Hagané*, 1997, vol. 83 (1), pp. 30-35.
18. S. Taniguchi and J.K. Brimacombe: *Iron Steel Inst. Jpn. Int.*, 1994, vol. 34, pp. 722-31.
19. N. El-Kaddah: *Conf. Records of IEEE on Industrial Applications*, IEEE, Piscataway, NJ, 1988, pp. 1162-67.
20. D. Shu, B.D. Sun, J. Wang, T.X. Li, and Y.H. Zhou: *Metall. Mater. Trans. A*, 1999, vol. 30A, pp. 2979-88.
21. P. Marty and A. Alemany: *Proc. Symp. of the IUTAM*, The Metals Society, London, 1982, pp. 245-59.
22. V.M. Korovin: *Magnetohydrodynamics*, 1988, vol. 24, pp. 160-65.